ELSEVIER

Journal of Hazardous Materials B73 (2000) 143–160

Journal of Hazardous Materials

www.elsevier.nl/locate/jhazmat

Experimental investigation into the incineration of wool scouring sludges in a novel rotating fluidised bed

W.Y. Wong [a,*], Y. Lu [a], V.S. Nasserzadeh [a], J. Swithenbank [a], T. Shaw [b,1], M. Madden [b,1]

[a] *Department of Chemical and Process Engineering, Sheffield University Waste Incineration Centre (SUWIC), University of Sheffield, Mappin Street, Sheffield S1 3JD, UK*

[b] *ENCO Development Centre (Wool Scouring Association), Valley Drive, Ilkley, West Yorkshire LS 298PB, UK*

Received 25 June 1999; received in revised form 19 October 1999; accepted 20 October 1999

Abstract

The main purpose of this research was to investigate the possibility of incineration of wool scouring sludges in a novel vertical axis rotating fluidised bed (RFB). A small-scale RFB was designed and constructed with an internal diameter (ID) of 200 mm and height of 50 mm to carry out the experiments. In phase one of the experiments, a cold test was conducted to investigate the fluidisation performance of the RFB, which eventually led to the optimisation of the operating parameters, i.e., sand particle size, rotation speed and bed loading (bed thickness) which ensures complete fluidisation and minimum particle elutriation. Sand particle size of 0.5 to 0.6 mm, rotation speed of 200 to 400 rpm and bed loading of 1 kg (equivalent to bed thickness of 27 mm) were found optimal. These information generated were useful for the second phase of the experiments, which was the hot test, in investigating the possibility of incinerating wool scouring sludges in the RFB. Nine wool sludges from different process routes generated from the wool scouring industries were analysed for their compositions. Most of these sludges were highly moist, had high volatile matter and high ash content with low level of fixed carbon. These characteristics made incineration difficult. Hence, the effect of varying the moisture content, rotation speed and sludge feed rate on the incineration of the three selected sludges were studied in the hot test. With 5% support methane, all sludges with a maximum moisture up to 70% as-received could be successfully burned in the RFB at rotating speeds of 200 and 300 rpm. The combustion was found

* Corresponding author. Tel.: +44-114-222-7500; fax: +44-114-222-7501; e-mail: mep98wyw@sheffield.ac.uk

[1] Tel.: +44-194-3601-555; fax: +44-194-3811-211.

PII: S0304-3894(99)00171-5

to be intense with a high efficiency due to the good turbulence and mixing in the RFB. The combustion gases produced, i.e., CO, CO_2 and NO_x were reasonably low due to the high combustion intensity and efficiency. To study the dynamics of the bed and freeboard region in the RFB, the velocity flow field was simulated using a computational fluid dynamics (CFD) model to generate information of the flow pattern. The special advantages of swirling flow would benefit the gas combustion in the RFB. The experimental results obtained have suggested that the incineration was successful and the ash particles elutriated were fine due to the good mixing and turbulence in the RFB. This also reflects the RFB as an effective incinerator.

Keywords: Rotating fluidised bed; Fluidisation; Wool scouring sludges; Waste incineration; Computational fluid dynamics

1. Introduction

In a rotating fluidised bed (RFB), the bed particles are introduced into the rotating cylindrical container with a porous wall that rotates around its axis of symmetry. The porous wall serves as the gas distributor, and the gas flows radially inward through it and through the bed particles. The bed particles are forced to the wall due to the large centrifugal forces produced by rotation and are balanced by the drag forces caused by the gas entering the porous wall. When these forces balance each other, the bed becomes fluidised. The minimum fluidisation condition in an RFB can be achieved at any gas flow rate by changing the rotating speed of the bed. This permits a much higher gas flow rate per unit area of the distributor than is possible in a conventional fluidised bed, which operates only against the vertical force of gravity. The gas flow passing through the bed can be increased proportionally to the g level produced by the rotation. In addition, the RFB provides an intensely turbulent intimate mixing between particles and fluid, which is beneficial to gain a high combustion efficiency.

The understanding of the operation of RFB has been of interest to many researchers since these devices have important industrial applications such as in the coal combustion, waste incineration, drying and dust filtration. Kroger et al. [1] has analysed the flow in both packed and fluidised beds in a rotating system. Expressions were found for the shape of the bed as well as the distribution of particles in packed beds, having different size distributions and densities. This has led to the deduction of equations predicting the pressure drop and radial flow distribution. Chevray et al. [2] has reported the trajectories of bubbles and entrained particles in an RFB based on the equations expressing a balance among inertial, centrifugal, coriolis, gravity and drag forces. The solutions gave rise to important information on the behaviour of isolated bubbles, bubble swarms and elutriation characteristics of the RFB. Further work has been carried out by Chen [3] who first suggested, in a theoretical analysis, that fluidisation occurred layer by layer from the inner bed surface outward at increasing radius as the gas velocity was increased. This was a very significant and interesting phenomenon, and also was extremely important in the design of these fluidised beds. Kao and Preffer [4] then further investigated the work of Chen [3] with the consideration of the influence of bed

thickness in the pressure drop — minimum fluidising velocities characteristics. Takahashi et al. [5] and Fan et al. [6] have also reported an interesting observation in their experiments which indicated a maximum in the pressure drop vs. velocity curve, instead of a plateau derived by Chen [3]. For its application in the waste incineration process, Swithenbank et al. [7] and Taib et al. [8] have demonstrated a novel RFB which has successfully incinerated sewage sludge with a high combustion efficiency and intensity. At Sheffield University Waste Incineration Centre (SUWIC), there are various research works currently carried out in RFB with different angles ranging from horizontal to vertical configurations, in which one of its applications was the incineration of waste.

The main purpose of this work was to generate the fundamental information based on those models proposed by the previous researchers on fluidisation characteristics, in order to design and operate a novel high efficiency RFB incinerator suitable for burning wool scouring sludges. Besides, a computational fluid dynamics (CFD) modelling was carried out to investigate the swirling effects on flow field in the RFB.

2. Experiment

2.1. Experimental rig

The small-scale RFB incinerator was designed and constructed. It consisted of an outer cylindrical vessel of 260 mm internal diameter (ID), which acted as a gas manifold to the co-axial 200 mm ID and 50 mm high air distributor cylinder. The air distributor cylinder was a stainless steel plate with 2-mm thickness and perforated with 0.5 mm diameter holes in a triangular pitch arrangement. The upper and bottom open ends were covered with 5-mm stainless steel plates, insulated with 10-mm thick refractory fire cement to withstand temperatures up to 1250°C. The central exit for the combustion gases was 80 mm ID located at the upper end plate. A 45° hood was installed at 80 mm above the central exit to collect the flue gas into the exhaust duct. The schematic diagram of the RFB is shown in Fig. 1. The whole assembly including the outer cylinder vessel rotated around its vertical axis of symmetry. A hollow drive shaft which was connected to a variable speed DC motor via a non-slip timing belt drove the rotation at speeds up to 1000 rpm ($100 \times g$ loading). The rotation speed was measured by a tachometer which counted the frequency of interruption of an infra-red signal generated by silver strips against a black background. Ten silver strips were used to count 10 disturbances that occurred for one revolution. Primary air was supplied by the compressor and fed through the hollow shaft of 34 mm ID into the RFB where the air flow rate was measured by two rotameters in parallel.

To begin the cold test experiment, the distributor pressure drop was first measured at an increasing air flow. Then, sand as the fluidisation material was charged into the bed through the central exit. The air flow rate was initially set at about 200 l/min while the rotation was set at a desired speed. The air flow was gradually increased and the total pressure drop was measured at the corresponding air flow rates. The bubbling action which began with the surface minimum U_{mfs} and critical minimum U_{mfc} fluidisation was

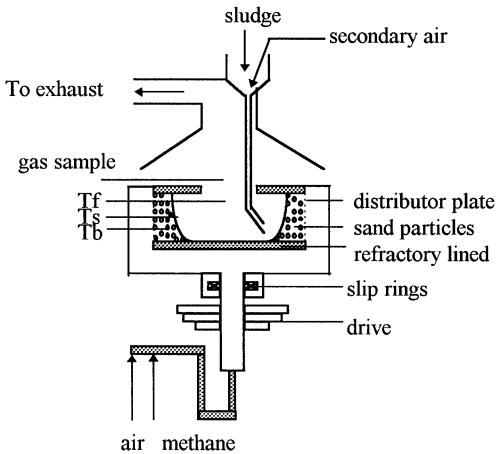

Fig. 1. The schematic diagram of the RFB combustor.

observed and recorded, together with the details about the bottom bed thickness, bed surface shapes, bubble eruptions and particle elutriation. The bed pressure drop measurement was obtained by subtracting the distributor pressure drop from the total pressure drop. The various operating parameters in this experiment are shown in Table 1.

To run the hot test, the air flow was set at a level which gave 2.5 U_{mfc} within the bed temperature of 850–1000°C, together with the corresponding rotation speed. The bed was ignited with a methane gas torch to preheat the bed to a stable temperature of 700–800°C. When the bed has reached uniform temperature, the sludge was fed into the bed from the exhaust end through a stainless steel feeding tube of 30 mm ID with a 100-mm opening. Secondary air was supplied to enhance the combustion as well as to pneumatically drive the sludge into the bed. The feed rate of sludge was controlled by feeding every 10 s, simulating a continuous feeding system. The operating conditions are summarised in Table 2.

For the temperature monitoring system, the bed of sand particles was equipped with four chromel/alumel (type K) thermocouples, located at the freeboard, bed surface, near the distributor (5 mm away from the distributor at middle height) and inside the bed (15 mm away from the distributor at middle height), respectively. All the thermocouples were connected via a rotating metal slip ring assembly through fixed metal tips to conduct the voltage signal for measurement. For the gas monitoring system, a simple stainless steel probe positioned at the combustor exit was used to extract samples of the

Table 1
The operating parameters varied in the cold test experiment

Sand size (mm)	0.85–1.00	0.71–0.85	0.50–0.60	0.30–0.43
Bed loading (kg)	1.5	1.0	0.5	
Rotation speeds (rpm)	400	300	200	100

Table 2
The operating conditions of the experiment

Sand size	0.5–0.6 mm
Rotation speeds	200–300 rpm
Bed loading	1 kg (27 mm bed thickness)
Bed temperature	800–950°C
Bed pressure drop	1.5–3 kPa
Fluidisation	$2.5U_{mfc}$
Air flow rate	600–720 g/min
CH_4 flow rate	146–178 g/min
Sludge feed rate	50–130 g/min

flue gas. The flue gas samples were split by a T-tube with one part being sent to the on-line CO_2 analyser (ADC non-dispersive infra-red absorption spectrometry analyser) and O_2/CO analyser (Servomex Xentra 4902 Continuous Emissions Paramagnetic Analyser), while the other part of the flue gas was sent through the heated line into the NO_x analyser (AAL Model 443 Chemiluminescent Analyser). All the above current or voltage signals were connected to a 16-channel data logger and displayed by an on-line PC computer.

2.2. Wool sludge samples

Nine wool sludge samples, which were collected from different wool scouring process routes with different chemical additives, were analysed. The compositions of these sludges varied from each other. Based on the related regulation in BS 1016, the proximate and ultimate analyses of these samples were determined. In addition, heavy metal contents were determined by inductively coupled plasma emission spectrometry and atomic absorption spectrometry after sample digestion using acid. Table 3 shows the results.

There was a certain degree of variation in the compositions of the wool scouring sludges. Generally, the sludges had a high volatile matter content and low fixed carbon, along with a high content of ash. The calorific values vary from 12 to 27 MJ/kg whereby the higher value may enable a self-sustaining combustion process. However, the high level of volatile matter indicated that most of the calorific value will be released in the combustion of the volatiles. The burning of volatiles tends to release most heat into the freeboard, i.e. less heat in the bed region to support combustion. The moisture content contributed to about 50–70% in most sludges. High moisture sludge will remove a lot of energy from the bed upon evaporation, and hence will discourage the sustainability of combustion. Sludges with a high ash content will be difficult to incinerate as ash is a non-combustible matter. Also, a higher ash content will result in more severe pollution. The ultimate analysis showed that the nitrogen and chlorine contents of the samples were comparatively low. The low level of nitrogen indicated that the sludges corresponded to low fuel-N compounds, thus nitrogen oxide emission will be low. The low chlorine content indicated that only low levels of dioxins will be produced. The heavy metals concentration showed a more distinct variation among those samples.

Table 3
Proximate and ultimate analysis of wool sludge samples

	A_2	B_2	C_2	D_2	E_2	F_2	G_2	I_2	J_2
Moisture, % w/w at 105°C	49.5	51.6	38.6	51.0	31.8	57.2	27.3	51.3	61.4
Analysis on sample dried at 105°C									
Volatile and fixed carbon, at 600°C, % w/w	43.3	68.5	66.3	83.8	57.4	72.6	54.2	72.7	63.0
Ash, % w/w	56.7	31.5	33.7	16.2	42.6	27.4	45.8	27.3	37.0
Carbon, % w/w	28.8	44.1	48.3	56.0	35.2	45.6	36.3	48.4	38.1
Hydrogen, % w/w	4.28	6.39	7.24	8.40	5.19	7.05	5.35	7.24	5.72
Nitrogen, % w/w	1.64	2.75	1.87	3.38	1.68	1.76	1.27	1.95	2.94
Chlorine, mg/kg	920	1140	4930	1240	550	2410	210	420	1510
Sulphur, mg/kg	1990	8010	2870	4470	4020	3390	2570	6670	4120
Calorific value, MJ/kg	12.53	21.05	19.07	27.01	18.99	22.74	17.24	22.42	17.70
pH value	4.9	6.9	9.3	4.6	4.3	6.4	3.8	7.7	5.9
Heavy metals, mg / kg									
Chromium	41	69	14	13	32	59	40	25	74
Nickel	13	11	< 5	< 5	7	11	10	9	12
Copper	37	32	29	27	33	44	23	16	32
Arsenic	11	4	5	5	< 3	23	< 3	11	15
Cadmium	7	< 1	< 1	< 1	< 1	3	< 1	< 1	1
Tin	< 5	< 5	< 5	< 5	< 5	< 5	< 5	< 5	< 5
Mercury	< 0.1	< 0.1	< 0.1	< 0.1	< 0.1	< 0.1	< 0.1	< 0.1	< 0.1
Lead	10	16	10	6	11	7	10	9	23
Manganese	340	130	160	69	55	250	47	470	280
Zinc	240	130	150	210	37	240	27	190	320

The results of the proximate and ultimate analyses are important as an indication of the possibility of incineration process and the levels of pollutants generated from the combustion products.

3. Experimental results and discussion

3.1. Cold test

3.1.1. Fluidisation and bed pressure drop

The bed pressure drop vs. air velocity diagram is clearly shown in Fig. 2 as an indication of the fluidisation performance of the RFB. The discrete points represented the experimental data points while the solid curves represented the theoretical predictions based on the theoretical model proposed by Kao and Preffer [4]. The experimental data points and the theoretical predictions showed close agreement to each other. However, the predictions were slightly higher than the actually observed over a wide range of gas velocity at these four rotating speeds. This was due to the assumption used in the theory that the bed exhibited a cylindrical shape and its axial thickness was uniform. In fact, the bed surface was parabolic, hence the gas flowed more freely through the upper bed which caused the pressure drop to be lower than the theoretical predictions.

The pressure drop curve as shown in Fig. 2 exhibited three stages. The first stage was the packed bed, its pressure drop depended almost linearly on the velocity. At the second stage, the bed was partially fluidised and the pressure drop exhibited a smooth curve which levelled off to a plateau. At the third stage, the bed reached the complete fluidisation, and the pressure drop was nearly constant. In the literature, there are two types of pressure drop vs. gas superficial velocity reported [5,6], these results however exhibited a plateau instead of a peak.

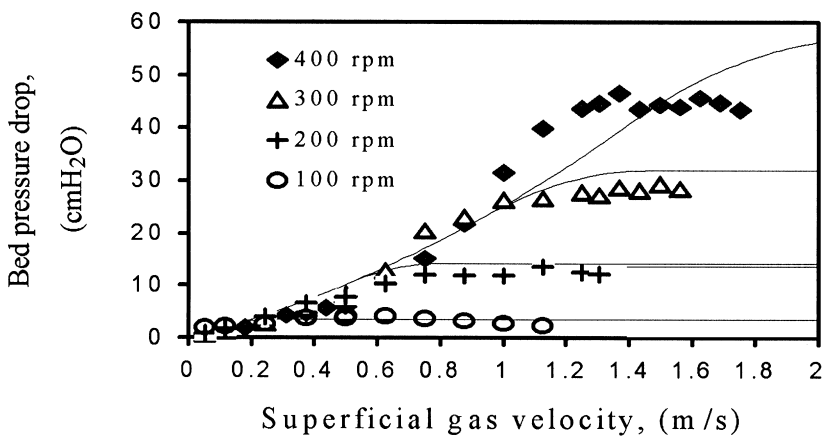

Fig. 2. Pressure drop vs. air velocity curves (1 kg sand, diameter 0.5–0.6 mm).

The bed surface shapes exhibited were dependent on the rotating speed of the RFB. At a higher rotating speed ($\geq$ 400 rpm), the bed surface took shape of a cylindrical annulus while at a lower rotating speed ($\leq$ 100 rpm), it exhibited a platform shape where the bed was thicker at the bottom by about 5–10 mm. Between these two speeds, the bed surface exhibited a parabola of revolution. Due to the platform shape of the bed surface ($\leq$ 100 rpm), there was a tendency for more gas flow to percolate through the upper part of bed, hence bubbles formed quicker at the upper bed which was thinner, while the bottom bed still remained a fixed bed until total fluidisation was reached. In order to achieve a uniform gas distribution, a relatively high pressure drop through the distributor was necessary to enhance its ratio to bed pressure drop, so that the localised fluidisation and consequent poor bed mixing could be avoided.

3.1.2. Optimisation of operating parameters

The various operating parameters tested in the cold test experiment, as shown in Table 1, have suggested their effect on the fluidisation characteristics in the RFB. In terms of rotating speed, a more uniform, cylindrical annulus bed surface shape was established at higher speed of 400 rpm (equivalent to $18 \times g$). This improved the air flow distribution inside the bed but the coalescence of bubbles was serious. The size of bubbles became large as the bubbles were subjected to deformation due to the high centrifugal force. At lower rotating speeds, bubbles eruptions occurred with some sand particles splashed out of the bed. In the case of the lowest rotating speed (100 rpm), the fluidisation was first initiated at a very low velocity with a platform shape of the bed surface. This resulted in the narrow region of air flow and poor bed mixing. Hence, the rotating speeds of 200–300 rpm were adopted in the following hot test.

Sand particle size had an effect on the fluidisation velocity, bubble size and bubble formation in the bed. A particle size of 0.5–0.6 mm was found optimal for good fluidisation conditions. During the fluidisation at about $2.5U_{\mathrm{mfc}}$, many small bubbles were released uniformly throughout the whole bed and particle elutriation was mild even though the maximum available fluidising air flow was introduced. Bubbles of a small size and large quantity led to good particle mixing due to their eddy wake. Too fine a particle size was not suitable as the fine particles were severely elutriated even though the bubble formation was more intense.

Bed thickness (associated to bed loading) was another important parameter affecting fluidisation due to the fact that fluidisation occurred layer by layer from the inner bed surface outward at an increasing air velocity. Too thick a bed produced less but bigger size bubbles (between 15 and 25 mm) due to the longer time for contact between bubbles. In addition, particle elutriation was more significant due to the thicker bed which resulted in a decrease in the centrifugal force. However, too thin a bed was not sufficient to serve the purpose as a fluidisation medium in the combustion process. Thus, bed thickness of 27 mm, corresponding to 1 kg sand loading was found suitable.

3.2. Hot test

The incineration of the selected four samples were studied by varying the feed rate, moisture content and rotation speed. The effect of operating temperature on the

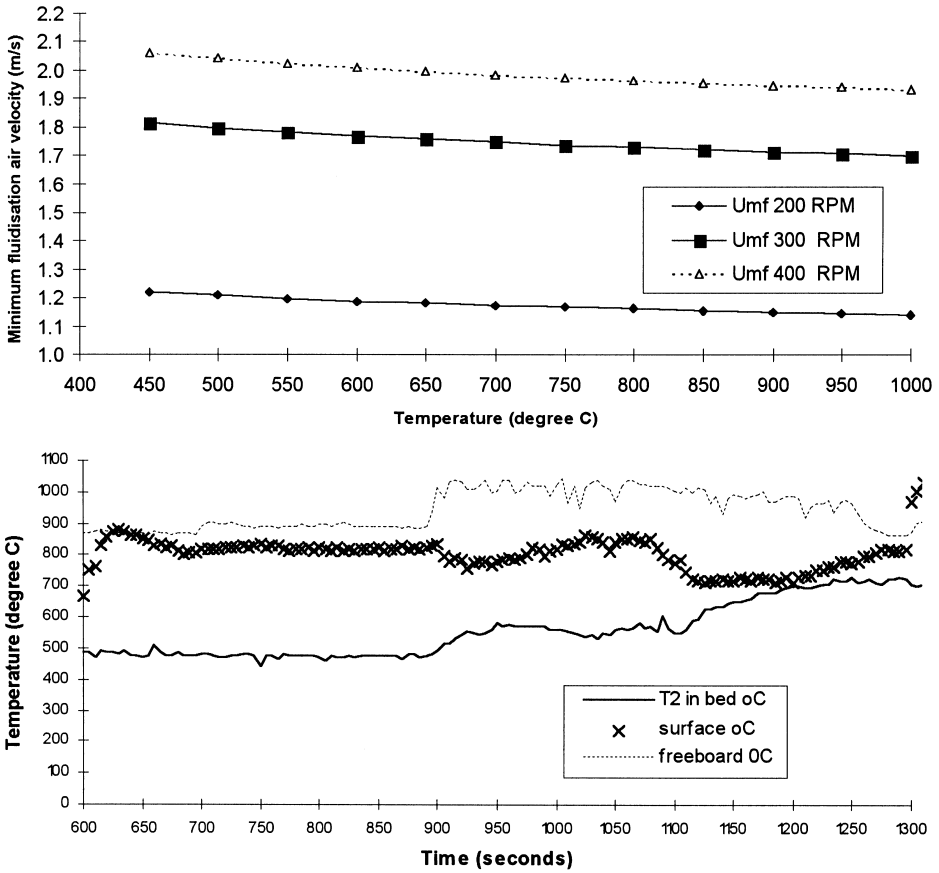

Fig. 3. Plot of minimum fluidisation air velocity required at a given elevated temperature.

minimum fluidisation velocity, U_{mf} changed the total air flow required in the hot test, for the same operation conditions used in the cold test. Fig. 3 shows the plot of minimum fluidisation air velocity required at a given elevated temperature. When the temperature of a bed changed, the properties of the fluidising fluid also changed, these in turn affected the U_{mf}. The fluidising air required at high temperature was less than required in the ambient temperature because of gas expansion. The increase in temperature will decrease the density of gas, ρ_f, but increase its viscosity, μ_f. Based on the proposal of Wu and Baeyens [9], at high Reynolds number where inertia effects predominated, it was expected that $U_{mf} \propto \rho_f$, hence $\approx T^{0.5}$. The density and viscosity of air at different temperature were evaluated from the following equations which predicted ρ_f and μ_f with maximum error of 1%.

$$\rho_f = 1.2 \times \frac{293}{T} \text{ and } \mu_f = \frac{1.46 \times 10^{-6} T^{1.504}}{T + 120}. \quad (1)$$

Thus, in order to calculate the air flow rate required for fluidisation at a given elevated temperature (in Kelvin), Eq. (2) is used.

$$U_{mf} \propto T^{0.5} \times \frac{T + 120}{T^{1.504}},$$

thus,

$$\frac{U_{mf1}}{U_{mf2}} = \frac{T_1^{0.5} \times \dfrac{T_1 + 120}{T_1^{1.504}}}{T_2^{0.5} \times \dfrac{T_2 + 120}{T_2^{1.504}}}. \quad (2)$$

3.2.1. Effect of sludge feed rates

Three feeding rates of sample A2, i.e. 50, 100 and 130 g/min were tested to determine the effects on the combustion and gas emissions. The in-situ temperature profile showed that a sludge feed rate of 50 g/min was completely incinerated with the methane support fuel, maintaining the bed temperature above 800°C. The freeboard temperature increased as the combustion of most volatiles took place in the freeboard with a long bright yellow flame. However, for 100 and 130 g/min sludge feed rates, the bed surface temperature showed a rapid decline due to the evaporation process took place at the bed surface. At freeboard temperature between 900°C and 1050°C for both feed rates, the sludge has successfully incinerated, revealing that the increase of heat released could offset the heat demand from evaporating the higher moisture at higher sludge feed rates. The combustion results under these different sludge feed rates are listed in Table 4.

3.2.2. Effect of sludge moisture content

Sample J2 was incinerated as-received (70% moisture) and after partial drying (32% moisture) with the feed rates of 70 and 31 g/min, respectively, to maintain the same amount of dry solids. The incineration of 70% moisture sludge failed as soon as the sludge feeding started. All the temperatures decreased rapidly and the fire eventually extinguished. This indicated that moisture evaporation absorbed so much heat that the bed temperature decreased rapidly before the effective devolatilisation of sludge could

Table 4
Incineration of sample A2

Feed rate, g/min	50	100	130
Air–fuel ratio	1.63	1.27	1.12
Combustion efficiency, %	88.3	87.9	86.4
Thermal efficiency, %	57.5	55.1	54.1
O_2, %	10.2	8.5	5.4
CO_2, %	6.2	7.3	9.3
CO, %	0.28	0.47	0.82
NO_x, ppm	302.9	497.2	509.6

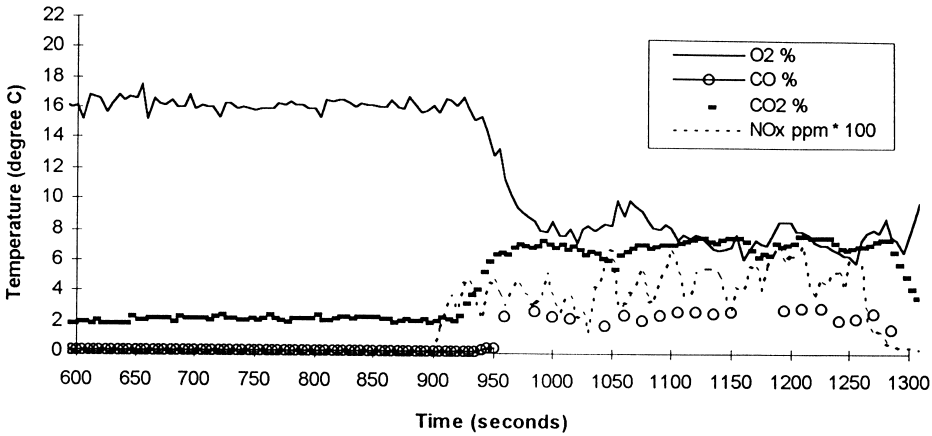

Fig. 4. The temperature profile and gas emissions of a partial dried 32% moisture sludge (sample J2), feed rate 31 g/min at 200 rpm, air flow rate 600 g/min, CH_4 146 g/min and started feeding at 895 s.

occur. With the sample being partially dried to 32% moisture, the incineration was successful. The temperature at the bed surface fluctuated slightly at 700–800°C and the freeboard temperature at 970–1050°C. The temperature profile and gas emissions of 32% moisture sludge are further illustrated in Fig. 4. The combustion efficiency was high at a value near 90%. The mass balance of carbon consumption and production of carbon dioxide and carbon monoxide presented the combustion efficiency. The thermal efficiency, however, was low at 48% due to the small amount of heat contained in the bed. Both the combustion and thermal efficiency calculations can be found in Appendix A. The gas emissions measurement showed that CO concentration was quite high (3.0%), indicating the incomplete combustion in the bed for this sample. This was mainly due to the rapid devolatilisation of the sample and insufficient air supply, which agreed with the devolatilisation test in the muffle furnace. However, it was found that most of the sludge had burned out in the bed, leaving fine ash particles after burning.

3.2.3. Effects of rotating speed

Rotating speeds of 200 and 300 rpm, equivalent to $4.5 \times g$ and $10 \times g$, respectively, were investigated for sample D2. At 200 rpm and 70 g/min of sludge feed rate, the bed temperature ranged from 750 to 800°C, and the freeboard temperature was maintained around 1000°C. The combustion was kept relatively constant as implied by the stable temperature profile. The incineration results are shown in Table 5. At a higher rotating

Table 5
Incineration of sample D2

Rotating speed, rpm	Air–fuel ratio	Combustion efficiency, %	Thermal efficiency, %	O_2, %	CO_2, %	CO, %	NO_x ppm
200	1.14	69.5	43.2	9.1	6.1	1.6	267.7
300	1.29	74.4	44.5	8.7	7.1	0.3	358.8

speed (300 rpm), an additional amount of sand was added to increase the bed thickness up to 33 mm in order to assist the fluidisation at the bed surface. Meanwhile, the air flow rate was slightly increased correspondingly. As the bed thickened, the thermocouple was buried into the bed and unable to show the local bed surface temperature where the incineration took place. However, from the visual observation, the sludge was successfully incinerated and the freeboard temperature remained at about 1050°C. Thus, the incineration of sludge at $10 \times g$ loading was possible in this RFB. The high rotating speed had increased combustion intensity, and due to the more turbulent mixing of the bed materials, the combustion and thermal efficiencies were improved.

4. CFD modelling of the RFB

4.1. Modelling approach

A domain of a quarter of the RFB was adopted employing a rotationally cyclic boundary of 90° angle. The computational grid was a 3-D geometry set-up, which contained a total of $10 \times 23 \times 30$ cells uniformly distributed circumferentially, radially and axially (I, J, K directions, respectively). The FLUENT code version 4.51 was used to compute the model. The conservation equations of mass, momentum and enthalpy were solved with the standard $k - \varepsilon$ turbulence model. The coriolis and centrifugal acceleration terms were added to the momentum equation arising from the additional acceleration since a rotating co-ordinate system is a non-inertial accelerating reference frame. Another momentum sink was added when the porous media model was activated. This porous model represented gas flow through the distributor plate and the bed of sand particles. During calculation, the angular wall velocity was set to be zero so that the wall would rotate at the same speed as the reference frame wall. The air flow entered the RFB uniformly around the distributor at a radial velocity of $2.5U_{\mathrm{mfc}}$ at a rotating speed of 200 rpm.

4.2. Results and discussion

4.2.1. Effect of rotation on the fluid flow in the RFB

The fluid emerging from the distributor plate (porous media) was moving radially inward with a tangential velocity component due to the rotation. The tangential velocity (W-Velocity) varied inversely with radius in order to maintain a constant angular momentum adjacent to the bed. The flow in this region was irrotational, similar to a free vortex flow. Near the axis of the rotation, the high velocity could no longer be sustained due to the viscous effects of the fluid, and a region of a solid body rotation was formed. The flow in this viscous core region was rotational and was referred to as the forced vortex flow, with the tangential velocity becoming zero at the axis of rotation. The tangential velocity profile is clearly illustrated in Fig. 5, where the inlet radial velocity was specified as $2.5U_{\mathrm{mfc}}$ of the 0.5–0.6 mm sand, both u and w inlet velocities were zero and the rotating speed was 200 rpm. As shown in Fig. 5, the interface of these two regions occurred at the radius of about 0.015 m, and the maximum tangential velocity

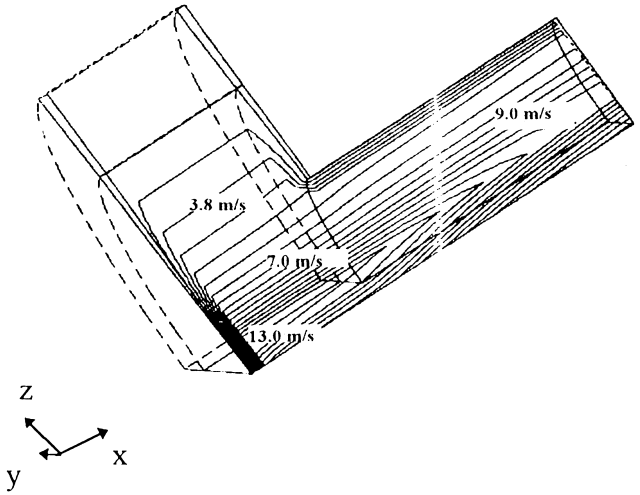

Fig. 5. Tangential velocity contours in the RFB (200 rpm, $2.5U_{mfc}$, 25°C).

was seen to be around 13.0 m/s. This fluid flow velocity pattern has confirmed the dynamics of the RFB. This velocity contours profile has also provided the required information to predict the temperature profile of the gas combustion in the RFB.

A semi-empirical analysis of flow in an RFB was carried out by Chevray et al. [2] based on the existing experimental data. With some assumptions and empirical correlation, the following equations were derived to estimate the tangential, radial and axial velocity:

In the irrotational zone, $r_m \le r \le r_i$,

$$w(r) = \frac{\omega r_i^2}{r}$$

$$v(r) = \frac{-Q}{2\pi rh}$$

$$u(r) = 0 \tag{3}$$

In the rotational zone, $0 \le r \le r_m$,

$$w(r) = \frac{100Q^2}{\omega\pi^2 r_i^4 h^2} r$$

$$v(r) = \frac{-Q}{2\pi r_m^2 h} r$$

$$u(r) = -\frac{Q}{\pi r_m^2 h} z \tag{4}$$

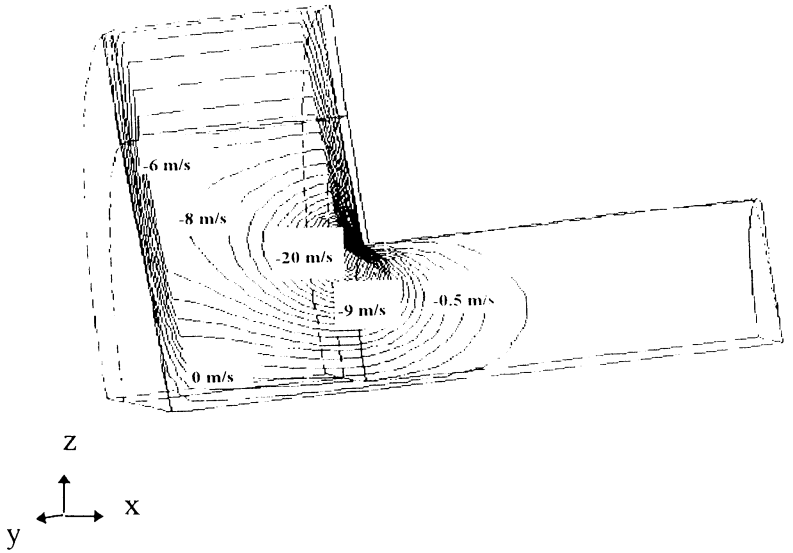

Fig. 6. Radial velocity contours in the RFB (200 rpm, $2.5U_{mfc}$, 25°C).

where Q is the air flow rate; h is the distributor height; r is the radial position; r_m, r_i are the viscous core radius and inner bed radius, respectively; u, v, w are the axial, radial and tangential velocity, respectively.

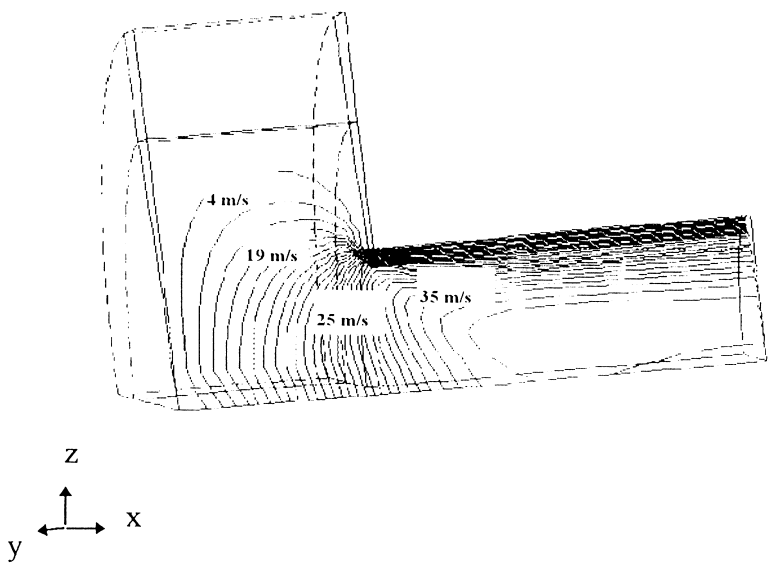

Fig. 7. Axial velocity contours in the RFB (200 rpm, $2.5U_{mfc}$, 25°C).

The CFD modelling of the radial and axial velocity in the RFB showed a similar result to the empirical analysis above, as shown in Figs. 6 and 7. The radial velocity (*V*-Velocity) in the irrotational zone was inversely proportional to the radial position inside the combustor. When the radius decreased, the cross-sectional area of the cylinder decreased. Thus, in order to conserve the volumetric flow rate of the air (assuming non-compressible flow), the radial velocity had to increase with the decreasing radial position. The axial velocity component (*U*-Velocity) was higher at the outlet region than at the bottom of the RFB, and reached a maximum at the outlet, as the flow was rushing out of the RFB at the exit port.

5. Conclusions

A novel vertical axis RFB incinerator was designed, constructed and operated at a small scale. The fluidisation performance of the RFB such as the bubbling, bed shape and pressure drop was studied with the determination of the optimum operating parameters, i.e., bed loading of 1 kg (equivalent to 27-mm bed thickness), sand particle size of 0.5–0.6 mm, and rotating speed between 200 and 400 rpm. These operating conditions were selected based on their low particle elutriation and improved bubble coalescence and formation. Nine wool scouring sludges were analysed and their compositions were reported. Most of these sludges were highly moist, had high volatile matter, and ash content but with low fixed carbon. Three sludge samples were selected for the incineration test. The effects of sludge feed rate, moisture content and rotating speed on the sludge combustion and gas pollutant emission were investigated. CFD analysis was carried out to further investigate the effects of swirling flow in the RFB. The calculated flow field showed two regions existing, i.e., the free vortex outer region and forced vortex flow near the axis. This special advantage of the swirling flow would benefit the incineration process due to its generation of turbulence which promotes mixing between particles and fluid. The experimental investigation of the fluidisation performance and incineration process has successfully reflected the RFB as an effective incinerator.

Nomenclature

Symbol	Descriptions, unit
h	Height of bed, m
Q	Volumetric flow rate of gas, m^3/s
r	Radial co-ordinate, m
r_i	Inner bed radius, m
r_m	Viscous core radius, m
U_{mf}	Minimum fluidising velocity, m/s
U_{mfc}	Critical minimum fluidising velocity, m/s
U_{mfs}	Surface minimum fluidising velocity, m/s
u	Axial velocity, m/s

v	Radial velocity, m/s
w	Tangential velocity, m/s
z	Vertical position co-ordinate, m
Greek letters	
ρ_f	Air density, kg/m^3
μ_f	Air viscosity, N/m s
ω	Angular velocity, rad/s

Acknowledgements

We would like to thank the following organisations for their financial and technical support: Sheffield University and ENCO Development Centre (Wool Scouring Association), UK.

Appendix A. Measurement of combustion and thermal efficiency

A.1. Combustion efficiency

Not all the sludges burnt to completion. Carbon monoxide, unburned hydrocarbon (HC) gases and unburned carbon particles appeared in the exhaust gases, hence, the maximum possible amount of heat had not been liberated within the combustion system. Carbon loss through elutriation could be significant. Unburned carbon particles and heat carried away by the excess air were the biggest single contributors to loss of efficiency. The mass balance of carbon consumption and production of carbon dioxide and carbon monoxide, presents the combustion efficiency calculation. The percentage of carbon conversion can be estimated based on the carbon and oxygen balances, and the analysis of dry flue gas.

α represent the molar flow rate of oxygen supplied (mol O_2/min), including oxygen available in the fuel, which is present in the dry flue gas, thus discounting the oxygen supplied that will react with H to form H_2O:

$$\alpha = Q\frac{0.21 \times 273}{T_m \times 22.4} + \frac{F_O}{32} - \frac{F_H}{4} \tag{5}$$

where Q is the volumetric flow rate of air supplied (l/min), T_m is the temperature of the rotameter (in Kelvin), F_O and F_H are the mass flow rates (g/min) of oxygen and hydrogen, respectively, which is present in the sludge feeding into the incinerator. Assuming that all oxygen supplied is converted to CO_2 and CO, and let β be the molar flow rate (mol/min) of CO_2, CO and non-reacted O_2 in the dry flue gas

$$\alpha = Y_{CO_2} + 0.5Y_{CO} + Y_{O_2} \qquad \beta = Y_{CO_2} + Y_{CO} + Y_{O_2}. \tag{6}$$

Thus,

$$Y_{CO_2} = \frac{[CO_2]\beta}{[CO_2]+[CO]+[O_2]}, \; Y_{CO} = \frac{[CO]\beta}{[CO_2]+[CO]+[O_2]},$$

$$Y_{O_2} = \frac{[O_2]\beta}{[CO_2]+[CO]+[O_2]} \tag{7}$$

where [] represents the volume or mole percentage of the corresponding components in the dry flue gas. When substituting Eq. (7) into Eq. (6):

$$\alpha = \frac{\beta([CO_2]+0.5[CO]+[O_2])}{[CO_2]+[CO]+[O_2]}. \tag{8}$$

The estimated amount of carbon being converted into CO_2 and CO,

$$Y_{TC}\,(\text{mol C/min}) = Y_{CO} + Y_{CO_2}. \tag{9}$$

FC represents the mass flow rate of carbon being fed into the bed (g C/min), then

$$\eta_{CE} = \frac{12\,Y_{TC}}{F_C} \times 100 \tag{10}$$

where η_{CE} is the percentage of carbon fed into the incinerator that has been consumed to produce CO_2 and CO. It can be written as a function of the known dry flue gas percentage as follows:

$$\eta_{CE} = \frac{12\,\alpha([CO]+[CO_2])}{F_C([CO_2]+0.5[CO]+[O_2])} \times 100. \tag{11}$$

A.2. Thermal efficiency

A steady state heat balance of sludge incineration in a fluidised bed is given below:

$$M_f q = M_a CP_a(T_b - T_a) + M_w \lambda + M_w CP_{wv}(T_b - 100°C) + M_{ds} CP_{ds}(350–100°C) + M_v CP_v(T_b - 350°C) + M_{ca} CP_{ca}(T_b - 350°C) \tag{12}$$

where q is the heat liberated per unit mass of fuel fed into the bed (J/g), M_a, M_f, M_w, M_v and M_{ca} are the mass flow rates of air, fuel, water, volatile and residual char plus ash supplied to the bed (g/min), respectively. The moisture content, volatile, char and ash are based on the proximate analysis. λ is the heat required to evaporate the moisture (2500 J/g), CP_{wv} and CP_a are the heat capacities of water vapour (1.98 J/g °C) and air (1.04 J/g °C), both are assumed constant. CP_{ds} is the average heat capacity of dry sludge (2.82 J/g °C), CP_v is the average heat capacity of volatile matter (1.67 J/g °C). T_b and T_a are the temperature of the bed and inlet air in degrees Celsius, where T_a is approximately 20°C ambient temperature.

The percentage of heat released into the bed, thermal efficiency, η_{TE},

$$\eta_{TE} = \frac{q}{\text{NHV of the waste}} \times 100 \quad (13)$$

where HHV is the higher heating value or gross CV of the sludge (J/g).

References

[1] D.G. Kroger, E.K. Levy, J.C. Chen, Flow characteristics in packed and fluidized rotating beds, Powder Technology 24 (1979) 9–18.
[2] R. Chevray, Y.N.I. Chan, F.B. Hill, Dynamics of bubbles and entrained particles in the rotating fluidized bed, AIChE Journal 26 (3) (1980) 390–397.
[3] Y.M. Chen, Fundamentals of a centrifugal fluidized bed, AIChE Journal 33 (5) (1987) 722–728.
[4] J. Kao, R. Preffer, On partial fluidisation in rotating fluidized beds, Powder Technology 33 (5) (1987) 858–861.
[5] T. Takahashi, Z. Tanaka, A. Itoshima, L.T. Fan, Performance of a rotating fluidized bed, Journal of Chemical Engineering of Japan 17 (1984) 333–336.
[6] L.T. Fan, C.C. Chang, Y.S. Yu, Incipient fluidization condition for a centrifugal fluidized bed, AIChE Journal 31 (6), 999–1009.
[7] J. Swithenbank, V. Nasserzadeh, R. Taib, D. Stagg, D. Moore, M. Ward, J. Bone, Incineration of wastes in novel high-efficiency tumbling and rotating fluidized bed incinerator, Journal of Environmental Engineering 123 (10) (1997) 1047–1052.
[8] M.R. Taib, V. Nasserzadeh, J. Swithenbank, S. Basire, Process intensification of sewage sludge disposal, Proceedings of the 1st International Symposium on Incineration and Flue Gas Treatment Technologies, The University of Sheffield, Sheffield, July, 1997.
[9] S.Y. Wu, J. Baeyens, Effect of operating temperature on minimum fluidization velocity, Powder Technology 67 (1991) 217–220.